Quality Assessment of Deblocked Images

Changhoon Yim, *Member, IEEE*, and Alan Conrad Bovik, *Fellow, IEEE*

Abstract—**We study the efficiency of deblocking algorithms for improving visual signals degraded by blocking artifacts from compression. Rather than using only the perceptually questionable PSNR, we instead propose a block-sensitive index, named PSNR-B, that produces objective judgments that accord with observations. The PSNR-B modifies PSNR by including a blocking effect factor. We also use the perceptually significant SSIM index, which produces results largely in agreement with PSNR-B. Simulation results show that the PSNR-B results in better performance for quality assessment of deblocked images than PSNR and a well-known blockiness-specific index.**

Index Terms—**Blocking effect, deblocking, distortion, image quality assessment, quantization.**

I. INTRODUCTION

BLOCKING effects are common in block-based image and video compression systems. Blocking artifacts are more serious at low bit rates, where network bandwidths are limited. Significant research has been done on blocking artifact reduction [7]–[14]. Most blocking artifact reduction methods assume that the distorted image contains noticeable amount of blocking. The degree of blocking depends upon several parameters, the most important of which is the quantization step for lossy compression. Little research has done on comparing the perceptual quality of deblocked images. The recent advent of powerful modern image quality assessment (IQA) algorithms [1]–[5] that compare well with human subjectively makes this plausible. Here we investigate quality assessment of deblocked images, and in particular we study the effects of the quantization step of the measured quality of deblocked images. A deblocking filter can improve image quality in some aspects, but can reduce image quality in other regards.

We perform simulations on the quality assessment of deblocked images. We first perform simulations using the conventional peak signal-to-noise ratio (PSNR) quality metric and a state of the art quality index, the structural similarity (SSIM) [1] index. The PSNR does not capture subjective quality well when blocking artifacts are present. The SSIM metric is slightly more complex than the PSNR, but correlates highly with human subjectively.

We also propose a new deblocking quality index that is sensitive to blocking artifacts in deblocked images. We name this peak signal-to-noise ratio including blocking effects (PSNR-B). The simulation results show that the proposed PSNR-B correlates well with subjective quality and with the SSIM index, and performs much better than the PSNR.

We study a variety of image and video deblocking algorithms, including lowpass filtering, projection onto convex sets (POCS), and the H.264 in-loop filter. The image improvements afforded by these algorithms is measured using the PSNR, PSNR-B, and SSIM. Rather than relying on PSNR, which correlates poorly with subjective judgment, we utilize PSNR-B which is designed specifically to assess blocky and deblocked images (but has no proven perceptual significance) in conjunction with the SSIM index, which is perceptually significant, but has not been demonstrated on deblocked images.

Section II reviews the image quality assessment methods we will consider. In Section III, we consider the relationship between quantization step size and image quality. Section IV introduces a distortion change concept to analyze the effects of deblocking filters. In Section V, we propose a new deblocking quality index, PSNR-B. Sections VI and VII present the simulation results on quality assessment of deblocked images and videos. We present concluding remarks in Section VIII.

II. QUALITY ASSESSMENT

We consider the class of quality assessment (QA) methods that are full-reference (FR) QA, which compares the test (distorted) image with a reference (original) image. In this paper, the distorted images will ostensibly suffer from blocking artifacts or from the residual artifacts following deblocking.

A. PSNR

The simplest and most widely used FR QA metrics are the peak signal-to-noise ratio (PSNR) and the mean-squared error (MSE) [1], [3].

Let $\mathbf{x}$ and $\mathbf{y}$ represent the vectors of reference and test image signals, respectively. Let $\mathbf{e}$ be the vector of error signal between $\mathbf{x}$ and $\mathbf{y}$. If the number of pixels in an image is N, then

$$\text{MSE}(\mathbf{x}, \mathbf{y}) = \frac{1}{N} \sum_{i=1}^{N} e_i^2 = \frac{1}{N} \sum_{i=1}^{N} (x_i - y_i)^2 \qquad (1)$$

$$\text{PSNR}(\mathbf{x}, \mathbf{y}) = 10 \log_{10} \frac{255^2}{\text{MSE}(\mathbf{x}, \mathbf{y})}. \qquad (2)$$

The PSNR is an attractive QA metric since it is mathematically simple and has clear physical meaning. However, the PSNR does not correlate well with perceived visual quality [1], [3]–[6].

C. Yim is with the Department of Internet and Multimedia Engineering, Konkuk University, Seoul 143-701, Korea (e-mail: cyim@konkuk.ac.kr).

A. C. Bovik is with the Department of Electrical and Computer Engineering, The University of Texas at Austin, Austin, TX 78712 USA (e-mail: bovik@ece.utexas.edu).

B. SSIM

The structural similarity (SSIM) metric aims to measure quality by capturing the similarity of images [1]. A product of three aspects of similarity are measured: luminance, contrast, and structure. The luminance comparison function $l(\mathbf{x}, \mathbf{y})$ for reference image $\mathbf{x}$ and test image $\mathbf{y}$ is defined as

$$l(\mathbf{x}, \mathbf{y}) = \frac{2\mu_x\mu_y + C_1}{\mu_x^2 + \mu_y^2 + C_1} \tag{3}$$

where μ_x and μ_y are the mean values of $\mathbf{x}$ and $\mathbf{y}$, respectively, and C_1 is a stabilizing constant.

The contrast comparison function $c(\mathbf{x}, \mathbf{y})$ is defined similarly as

$$c(\mathbf{x}, \mathbf{y}) = \frac{2\sigma_x\sigma_y + C_2}{\sigma_x^2 + \sigma_y^2 + C_2} \tag{4}$$

where σ_x and σ_y are the standard deviation of $\mathbf{x}$ and $\mathbf{y}$, respectively, and C_2 is a stabilizing constant.

The structure comparison function $s(\mathbf{x}, \mathbf{y})$ is defined as

$$s(\mathbf{x}, \mathbf{y}) = \frac{\sigma_{xy} + C_3}{\sigma_x\sigma_y + C_3} \tag{5}$$

where σ_{xy} is the correlation between $\mathbf{x}$ and $\mathbf{y}$ and C_3 is also a constant that provides stability.

The SSIM index is obtained by combining the three comparison functions

$$\text{SSIM}(\mathbf{x}, \mathbf{y}) = [l(\mathbf{x}, \mathbf{y})]^\alpha \cdot [c(\mathbf{x}, \mathbf{y})]^\beta \cdot [s(\mathbf{x}, \mathbf{y})]^\gamma. \tag{6}$$

In [1], the parameters are set as $\alpha = \beta = \gamma = 1$ and $C_3 = C_2/2$

$$\text{SSIM}(\mathbf{x}, \mathbf{y}) = \frac{(2\mu_x\mu_y + C_1)(2\sigma_{xy} + C_2)}{\left(\mu_x^2 + \mu_y^2 + C_1\right)\left(\sigma_x^2 + \sigma_y^2 + C_2\right)}. \tag{7}$$

Local SSIM statistics are estimated using a symmetric Gaussian weighting function. The mean SSIM index pools the spatial SSIM values to evaluate the overall image quality [1]

$$\text{SSIM}(\mathbf{x}, \mathbf{y}) = \frac{1}{M} \sum_{j=1}^{M} \text{SSIM}(\mathbf{x}_j, \mathbf{y}_j) \tag{8}$$

where M is the number of local windows over the image, and $\mathbf{x}_j$ and $\mathbf{y}_j$ are image patches covered by the jth window.

III. QUANTIZATION STEP SIZE AND IMAGE QUALITY

Quantization is a key element of lossy compression, but information is lost. There is a tradeoff between compression ratio and reconstructed image/video quality. The amount of compression and the quality can be controlled by the quantization step. As the quantization step is increased, the compression ratio becomes larger, and the quality generally worsens. However, there has not been a study made of how perceptual quality suffers as a function of step size, or the degree to which deblocking augments perceptual quality. The emergence of new and powerful IQA indices suggests this possibility.

In block transform coding, the input image is divided into $L \times L$ blocks, and each block is transformed independently into
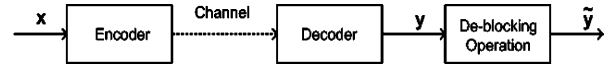

Fig. 1. Block diagram for reference, decoded, and deblocked images.

transform coefficients. An input image block b is transformed into a DCT coefficient block

$$B = TbT^t \tag{9}$$

where T is the transform matrix and T^t is the transpose matrix of T. The transform coefficients are quantized using a scalar quantizer Q

$$\tilde{B} = Q(B) = Q(TbT^t). \tag{10}$$

The quantization operator in (10) is nonlinear, and is a many-to-one mapping from R^{L^2} to R^{L^2} [7].

In the decoder, only quantized transform coefficients $\tilde{B}$ are available. The output of the decoder is

$$\tilde{b} = T^t\tilde{B}T = T^tQ(TbT^t)T. \tag{11}$$

Let Δ represent the quantization step. It is well known that the PSNR is a monotonically decreasing function of Δ.

The SSIM index captures the similarity of reference and test images. As the quantization step size becomes larger, the structural differences between reference and test image will generally increase, and in particular the structure term $s(\mathbf{x}, \mathbf{y})$ in (5) will become smaller. Hence, the SSIM index would be a monotonically decreasing function of the quantization step size Δ.

IV. DEBLOCKING FILTER AND DISTORTION CHANGE

As before, $\mathbf{x}$ is the reference (original) image and $\mathbf{y}$ is the decoded image that has been distorted by quantization errors. Let $\tilde{\mathbf{y}}$ represent the deblocked image and f represent the deblocking operation: $\tilde{\mathbf{y}} = f(\mathbf{y})$. Fig. 1 shows a block diagram depicting the flow of reference, decoded, and deblocked images. Let $M(\mathbf{x}, \mathbf{y})$ be the quality metric between $\mathbf{x}$ and $\mathbf{y}$. The goal of the deblocking operation f is to maximize $M(\mathbf{x}, f(\mathbf{y}))$, given image $\mathbf{y}$.

Deblocking is a local operation. The deblocking operation may improve the appearance of the image in some regions, while degrading the quality elsewhere.

Let $d(x_i, y_i)$ be the distortion between the ith pixels of $\mathbf{x}$ and $\mathbf{y}$, expressed as squared Euclidean distance

$$d(x_i, y_i) = \|x_i - y_i\|^2. \tag{12}$$

Next, we define the distortion decrease region (DDR) $\mathcal{A}$ to be composed of those pixels where the distortion is decreased by the deblocking operation

$$i \in \mathcal{A}, \text{ if } d(x_i, \tilde{y}_i) < d(x_i, y_i).$$

The amount of distortion decrease for the ith pixel α_i in the DDR $\mathcal{A}$ is

$$\alpha_i = d(x_i, y_i) - d(x_i, \tilde{y}_i). \tag{13}$$

The distortion may also increase at other pixels by application of the deblocking filter. We similarly define the distortion increase region (DIR) $\mathcal{B}$

$$i \in \mathcal{B}, \text{ if } d(x_i, y_i) < d(x_i, \tilde{y}_i).$$

The amount of distortion increase for the ith pixel β_i in the DIR $\mathcal{B}$ is

$$\beta_i = d(x_i, \tilde{y}_i) - d(x_i, y_i). \tag{14}$$

We define the mean distortion decrease (MDD)

$$\bar{\alpha} = \frac{1}{N} \sum_{i \in \mathcal{A}} (d(x_i, y_i) - d(x_i, \tilde{y}_i)) \tag{15}$$

where N is the number of pixels in the image. Similarly the mean distortion increase (MDI) is

$$\bar{\beta} = \frac{1}{N} \sum_{i \in \mathcal{B}} (d(x_i, \tilde{y}_i) - d(x_i, y_i)). \tag{16}$$

A reasonable approach for designing a deblocking filter would be to seek to maximize the MDD $\bar{\alpha}$ and minimize the MDI $\bar{\beta}$. This is generally a very difficult task and of course, may not result in optimized improvement in perceptual quality.

Lastly, let $\bar{\gamma}$ be the mean distortion change (MDC), defined as the difference between MDD and MDI

$$\bar{\gamma} = \bar{\alpha} - \bar{\beta}. \tag{17}$$

If $\bar{\gamma} < 0$, then the deblocking operation is likely unsuccessful since the mean distortion increase is larger than the mean distortion decrease. We would expect a successful deblocking operation to yield $\bar{\gamma} > 0$. Nevertheless, these conditions are not equated with levels of perceptual improvement or loss.

Deblocking can be considered as an image restoration problem. Let g represent the deblocking operation function and $\mathcal{N}(x_i)$ represent a neighborhood of pixel x_i.

A lowpass filter is a simple deblocking filter. An $L \times L$ lowpass filter can be represented as

$$g(\mathcal{N}(x_i)) = \sum_{k=1}^{L^2} h_k \cdot x_{i,k} \tag{18}$$

where h_k is the kernel for the $L \times L$ filter and $x_{i,k}$ is the kth pixel in the $L \times L$ neighborhood of pixel x_i.

While lowpass filtering does reduce blocking artifacts, critical high frequency information is also lost and the image is blurred. While the distortion will certainly decrease for some pixels that define the DDR $\mathcal{A}$, the distortion will likely increase for a significant number of pixels in DIR $\mathcal{B}$. Indeed, it is quite possible that $\bar{\gamma} < 0$ could result. Moreover, blur is perceptually annoying.

A variety of nonlinear methods have been proposed to reduce the blocking artifacts, while minimizing the loss of original information [7]–[14]. For example, deblocking algorithms based upon projection onto convex sets (POCS) have demonstrated good performance for reducing blocking artifacts and

have proved popular [7]–[12]. In POCS, a lowpass filtering operation is performed in the spatial domain, while a projection operation is performed in the DCT domain. Typically, the projection operation is a clipping operation on the filtered coefficients, confining these to fall within a certain range defined by the quantization step size.

Since the lowpass filtering and the projection operations are performed in different domains, forward DCT and inverse DCT (IDCT) operations are required. The lowpass filtering, DCT, projection, IDCT operations compose one iteration, and multiple iterations are required to achieve convergence. It is argued that under certain conditions, POCS filtered images converge to an image that does not exhibit blocking artifacts [7], [10], [11].

As another example, the H.264 in-loop deblocking filter is a key component in the H.264 video coding standard [17]. It is claimed that the in-loop filtering significantly improves both subjective and objective video quality [15]. The key idea of the H.264 in-loop filter is to adaptively select the filtering operation g and the neighborhood $\mathcal{N}(x_i)$ using the relative pixel location with respect to the block boundary and the local gray level gradient information. Generally, the MDI $\bar{\beta}$ value is reduced while the MDD $\bar{\alpha}$ value is similar to lowpass filtering.

The H.264 in-loop filter uses separate 1-D operations and integer multiplications to reduce complexity. However, it still requires a large amount of computation. In fact, the H.264 in-loop filter requires about one-third of the computational complexity of the decoder [15].

V. PSNR INCLUDING BLOCKING EFFECTS

In the following, we propose a new block-sensitive image quality metric which we term peak signal-to-noise ratio including blocking effects (PSNR-B). As the quantization step size increases, blocking artifacts generally become more conspicuous. Blocking artifacts are gray level discontinuities at block boundaries, which are ordinarily oriented horizontally and vertically. They arise from poor representation of the block luminance levels near the block boundaries [24].

The following definitions are relative to an assumed block-based compression tiling, e.g., 8×8 blocks as in JPEG compression. For simplicity, assume that an integer number of blocks comprise the image, viz., that horizontal and vertical dimensions are divisible by the block dimension. The definitions apply whether the image is compressed, not-compressed, or deblocked following decompression.

We, therefore, consider blocking artifacts that occur along the horizontal and vertical orientations. Let N_H and N_V be the horizontal and vertical dimensions of the $N_H \times N_V$ image I. Let $\mathcal{H}$ be the set of horizontal neighboring pixel pairs in I. Let $\mathcal{H}_B \subset \mathcal{H}$ be the set of horizontal neighboring pixel pairs that lie across a block boundary. Let $\mathcal{H}_B^C$ be the set of horizontal neighboring pixel pairs, not lying across a block boundary, i.e., $\mathcal{H}_B^C = \mathcal{H} - \mathcal{H}_B$. Similarly, let $\mathcal{V}$ be the set of vertical neighboring pixel pairs, and $\mathcal{V}_B$ be the set of vertical neighboring pixel pairs lying across block boundaries. Let $\mathcal{V}_B^C$ be the set of vertical neighboring pixel pairs not lying across block boundaries, i.e., $\mathcal{V}_B^C = \mathcal{V} - \mathcal{V}_B$.

y_1	y_2	y_3	y_4	y_5	y_6	y_7	y_8
y_9	y_{10}	y_{11}	y_{12}	y_{13}	y_{14}	y_{15}	y_{16}
y_{17}	y_{18}	y_{19}	y_{20}	y_{21}	y_{22}	y_{23}	y_{24}
y_{25}	y_{26}	y_{27}	y_{28}	y_{29}	y_{30}	y_{31}	y_{32}
y_{33}	y_{34}	y_{35}	y_{36}	y_{37}	y_{38}	y_{39}	y_{40}
y_{41}	y_{42}	y_{43}	y_{44}	y_{45}	y_{46}	y_{47}	y_{48}
y_{49}	y_{50}	y_{51}	y_{52}	y_{53}	y_{54}	y_{55}	y_{56}
y_{57}	y_{58}	y_{59}	y_{60}	y_{61}	y_{62}	y_{63}	y_{64}

Fig. 2. Example for illustration of pixel blocks.

Let N_{H_B}, $N_{H_B^C}$, N_{V_B}, and $N_{V_B^C}$ be the number of pixel pairs in $\mathcal{H}_B$, $\mathcal{H}_B^C$, $\mathcal{V}_B$, and $\mathcal{V}_B^C$, respectively. If B is the block size, then

$$N_{H_B} = N_V \left(\frac{N_H}{B} \right) - 1$$
$$N_{H_B^C} = N_V (N_H - 1) - N_{H_B}$$
$$N_{V_B} = N_H \left(\frac{N_V}{B} \right) - 1$$
$$N_{V_B^C} = N_H (N_V - 1) - N_{V_B}.$$

Fig. 2 shows a simple example for illustration of pixel blocks with $N_H = 8$, $N_V = 8$, and $B = 4$. The thick lines represent the block boundaries. In this example, $N_{H_B} = 8$, $N_{H_B^C} = 48$, $N_{V_B} = 8$, and $N_{V_B^C} = 48$. The sets of pixel pairs in this example are

$$\mathcal{H}_B = \{(y_4, y_5), (y_{12}, y_{13}), \ldots, (y_{60}, y_{61})\}$$
$$\mathcal{H}_B^C = \{(y_1, y_2), (y_2, y_3), (y_3, y_4), (y_5, y_6)$$
$$\ldots, (y_{63}, y_{64})\}$$
$$\mathcal{V}_B = \{(y_{25}, y_{33}), (y_{26}, y_{34}), \ldots, (y_{32}, y_{40})\}$$
$$\mathcal{V}_B^C = \{(y_1, y_9), (y_9, y_{17}), (y_{17}, y_{25}), (y_{33}, y_{41})$$
$$\ldots, (y_{56}, y_{64})\}.$$

Then we define the mean boundary pixel squared difference (D_B) and the mean nonboundary pixel squared difference (D_B^C) for image $\mathbf{y}$ to be

$$D_B(\mathbf{y}) = \frac{\sum\limits_{(y_i,y_j)\in\mathcal{H}_B} (y_i - y_j)^2 + \sum\limits_{(y_i,y_j)\in\mathcal{V}_B} (y_i - y_j)^2}{N_{H_B} + N_{V_B}} \quad (19)$$

$$D_B^C(\mathbf{y}) = \frac{\sum\limits_{(y_i,y_j)\in\mathcal{H}_B^C} (y_i - y_j)^2 + \sum\limits_{(y_i,y_j)\in\mathcal{V}_B^C} (y_i - y_j)^2}{N_{H_B^C} + N_{V_B^C}} . \quad (20)$$

Generally, as the quantization step size increases, D_B will increase relative to D_B^C, and blocking artifacts will become more visible. Of course, this does not establish any level of correlation between (19), (20) and perceptual annoyance.

Also define the blocking effect factor

$$\text{BEF}(\mathbf{y}) = \eta \cdot \left[D_B(\mathbf{y}) - D_B^C(\mathbf{y}) \right] \quad (21)$$

where

$$\eta = \begin{cases} \frac{\log_2 B}{\log_2(\min(N_H, N_V))}, & \text{if } D_B(\mathbf{y}) > D_B^C(\mathbf{y}) \\ 0, & \text{otherwise} \end{cases} \quad (22)$$

emphasizes the BEF as a function of block size. The assumption here is that the visibility of blocking effects increases with block size.

Of course, there can be multiple block sizes in a particular decoded image/video. For example, there can be 16×16 macroblocks and 4×4 transform blocks, both contributing to blocking effects, as in H.264 video coding. Let D_{B_k}, $D_{B_k}^C$, BEF_k, and η_k modify (19)–(22) for block size B_k. Then

$$\text{BEF}_k(\mathbf{y}) = \eta_k \cdot \left[D_{B_k}(\mathbf{y}) - D_{B_k}^C(\mathbf{y}) \right]. \quad (23)$$

The BEF over all block sizes is defined as

$$\text{BEF}_{\text{Tot}}(\mathbf{y}) = \sum_{k=1}^{K} \text{BEF}_k(\mathbf{y}). \quad (24)$$

The mean-squared error including blocking effects (MSE-B) for reference image $\mathbf{x}$ and test image $\mathbf{y}$ is then defined as the sum of the $\text{MSE}(\mathbf{x}, \mathbf{y})$ in (1) and $\text{BEF}_{\text{Tot}}(\mathbf{y})$ in (24)

$$\text{MSE-}B(\mathbf{x}, \mathbf{y}) = \text{MSE}(\mathbf{x}, \mathbf{y}) + \text{BEF}_{\text{Tot}}(\mathbf{y}). \quad (25)$$

Finally, we propose the PSNR-B as

$$\text{PSNR-}B(\mathbf{x}, \mathbf{y}) = 10 \log_{10} \frac{255^2}{\text{MSE-}B(\mathbf{x}, \mathbf{y})}. \quad (26)$$

The MSE term in (25) measures the distortion between the reference image $\mathbf{x}$ and the test image $\mathbf{y}$, while the BEF term in (25) specifically measures the amount of blocking artifacts just using the test image $\mathbf{y}$. The BEF itself can be used as a no-reference quality index, similar to the generalized block-edge impairment metric (GBIM) [20] and the mean noticeable blockiness score (MNBS) [21]. These no-reference quality indices claim to be efficient for measuring the amount of blockiness, but may not be efficient for measuring image quality relative to full-reference quality assessment. On the other hand, the MSE is not specific to blocking effects, which can substantially affect subjective quality. We argue that the combination of MSE and BEF is an effective measurement for quality assessment considering both the distortions from the original image and the blocking effects in the test image. The associated quality index PSNR-B is obtained from the MSE-B by a logarithmic function, as is the PSNR from the MSE. The PSNR-B is attractive since it is specific for assessing image quality, specifically the severity of blocking artifacts.

VI. SIMULATION RESULTS ON DEBLOCKED IMAGES

This section presents simulation results on quality assessment of deblocked images. Images are compressed using DCT block coding as JPEG. In JPEG, quantization is applied using a different quantization step size for each DCT coefficient, as defined by a quantization table. Here, we apply the same quantization step size for all DCT coefficients, to more directly investigate the effects of quantization step size on image quality. This also
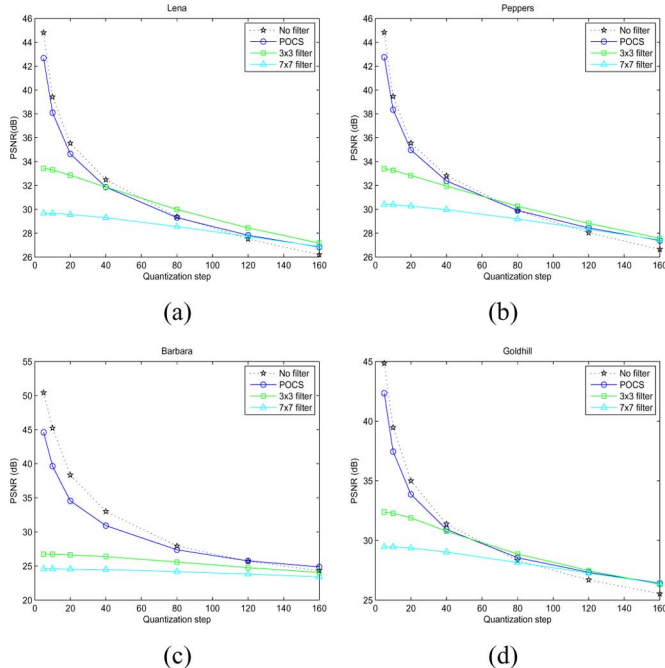
Fig. 3. PSNR comparison of images. (a) Lena. (b) Peppers. (c) Barbara. (d) Goldhill.

Fig. 4. SSIM comparison of images. (a) Lena. (b) Peppers. (c) Barbara. (d) Goldhill.

accords with the analysis of H.264 video in Section VII, since H.264 compression uses the same quantization step size for all transform coefficients as determined by the quantization parameter (QP). Quantization step sizes of 5, 10, 20, 40, 80, 120, and 160 were used in the simulations to investigate the effects of quantization step size. Deblocking was applied on the decoded images for comparison.

A. PSNR Analysis

Fig. 3 shows the comparison with respect to PSNR. When the quantization step size was large ($\Delta \geq 120$), the 3×3 filter, 7×7 filter, and POCS methods resulted in higher PSNR than the no-filter case on the Lena, Peppers, and Goldhill images. On the more complex Barbara image, all the methods resulted in similar PSNR values, while the POCS gave a slightly higher PSNR at $\Delta = 160$.

When the quantization step was small ($\Delta \leq 40$), all the deblocking methods produced lower PSNR compared to the no-filter case. The POCS did not produce improvement. When the quantization step is small, the MDI was larger than the MDD. In other words, the amount of information that was distorted was larger than the amount of information recovered by deblocking filters. When the quantization step size fell in the middle range of about 80, the 3×3 filter gave a slightly higher PSNR on the Lena, Peppers, and Goldhill images.

B. SSIM Analysis

Fig. 4 shows the result of comparing images using the well-known and perceptually significant SSIM index [1]. When the quantization step was large ($\Delta \geq 120$), all the filtering methods resulted in larger SSIM values on the Lena, Peppers, and Goldhill images. On the Barbara image, only POCS produced a larger
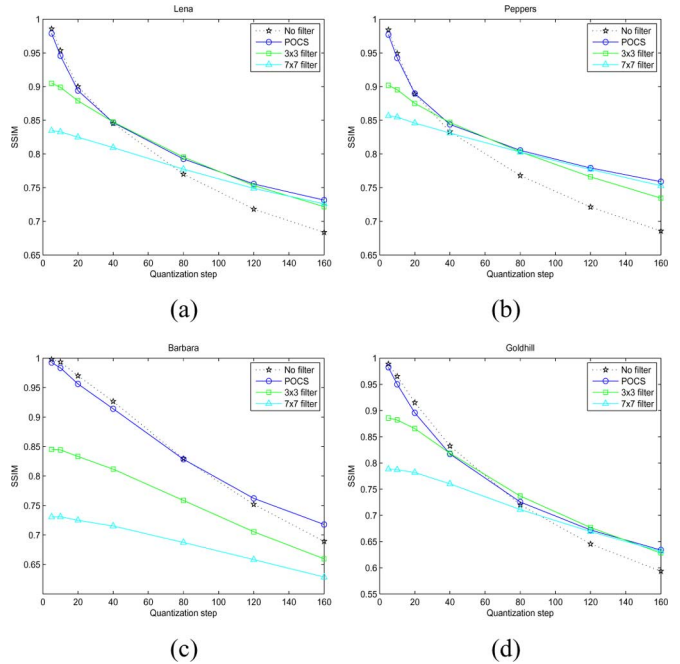
SSIM value than the no-filter case. When the quantization step size was small ($\Delta < 40$), the 3×3 and 7×7 lowpass filters resulted in lower SSIM values than the no-filter case, while the POCS method had little effect on the SSIM value. On the Peppers image, all the filtering methods produced much larger SSIM values at $\Delta = 80$, and slightly higher SSIM values at $\Delta = 40$, as compared to not filtering. On the Barbara image, only the POCS approach did not reduce the SSIM values, while the lowpass filtering methods gave much lower SSIM values than the no-filter case at quantization step 80. The Barbara image contains complex textures with high frequency components, yet the amount of information lost by lowpass filtering is significant.

C. GBIM Analysis

We performed simulations using a blockiness-specific quality index, the so-called generalized block-edge impairment metric (GBIM) in [20], for comparison. Fig. 5 shows the GBIM comparison of images. The GBIM is an overall ratio between the mean-weighted-squared pixel differences between pixel pairs lying across a block boundary and pixels pairs not lying across a block boundary. As shown in Fig. 5, GBIM becomes large when there are blocking effects. GBIM becomes very large as the quantization step increases when no filter is used. When any deblocking algorithm is applied, GBIM becomes much smaller than in the no-filter case even for large quantization steps. In this regard, the GBIM can be an effective index for measuring the amount of blockiness.

D. BEF Analysis

Fig. 6 shows the blocking effect factor (BEF) comparison of images. The BEF results in very similar trends as GBIM in Fig. 5. In Fig. 6, the BEF becomes quite large when no filter is applied for large quantization steps. All deblocking algorithms
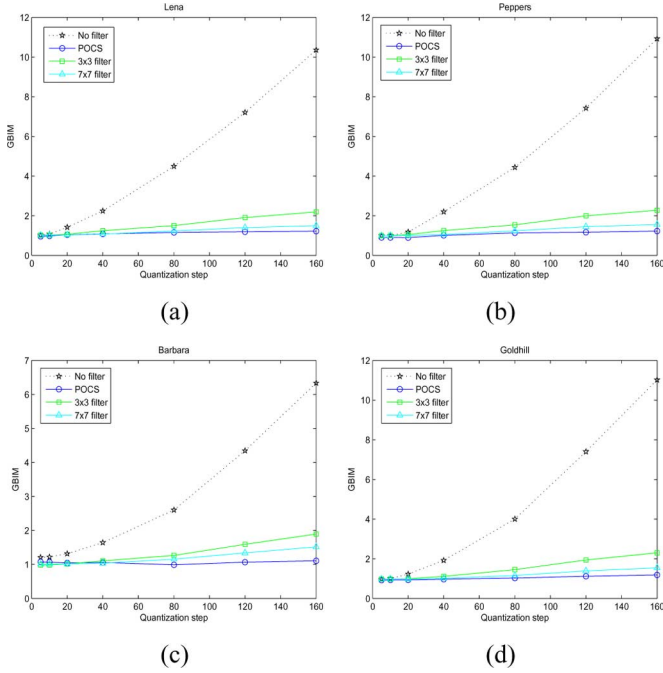
Fig. 5. GBIM comparison of images. (a) Lena. (b) Peppers. (c) Barbara. (d) Goldhill.
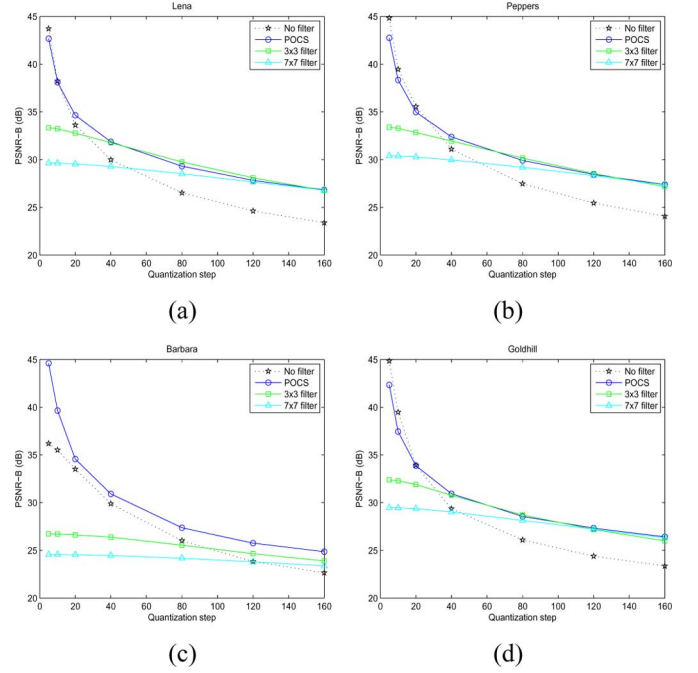

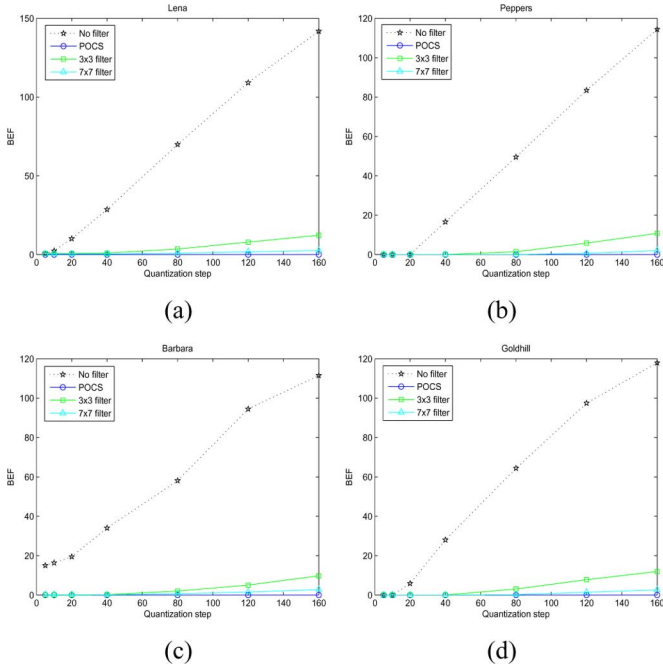Fig. 7. PSNR-B comparison. (a) Lena. (b) Peppers. (c) Barbara. (d) Goldhill.

Fig. 6. BEF comparison of images. (a) Lena. (b) Peppers. (c) Barbara. (d) Goldhill.

are effective for reducing BEF, and POCS removes the blocking effects very effectively in terms of BEF.

E. PSNR-B Analysis

Fig. 7 shows the comparison of deblocking algorithms using the distortion-specific PSNR-B index. For moderate to large range of quantization step sizes ($\Delta > 40$), POCS produced improved PSNR-B values relative to the no-filter case over all the images. For large quantization steps ($\Delta > 100$), the simple

lowpass filtering methods also improved the PSNR-B values on the Lena, Peppers, and Goldhill images. Since the local spatial variations are relatively larger in Barbara image, the BEF was relatively large even at small quantization steps in no-filter case. Hence, the POCS resulted in improved PSNR-B values compared to the no-filter case even at small quantization steps in Barbara image. Compared to PSNR, the PSNR-B improves more markedly on the deblocked images, especially for large quantization steps. The PSNR-B was largely in agreement with the SSIM index.

F. Subjective Quality Assessment Experiment

We performed a subjective quality assessment experiment. The experiment was based upon the double-stimulus impairment scale (DSIS) Variant I in ITU-R BT.500-11 [22]. The double-stimulus method is cyclic, wherein the original (reference) image is first presented, then the same impaired (distorted) image is presented. The DSIS Variant I presentation timing is as shown in Fig. 8.

After the presentation of the original image ($T1$) and the mid-gray image ($T2$), the observer votes while the impaired image ($T3$) or mid-gray image ($T4$) is presented. The observer is asked to vote the subjective impairment score (SIS) using the five-grade impairment scale in [22]:
1) imperceptible;
2) perceptible, but not annoying;
3) slightly annoying;
4) annoying;
5) very annoying.

The subjective impairment score ranges from 1 to 5, and we used a continuous scale for improved accuracy. In our experiment, the observers were not asked to vote specifically for the amount of blockiness nor for the amount of blur. They were just asked to vote their subjective judgment of impairment compared
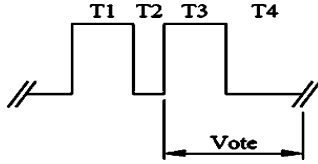
Fig. 8. DSIS Variant I presentation timing ($T1 = 10$ s original image, $T2 = 3$ s mid-gray image, $T3 = 10$ s impaired image, $T4 = 10$ s mid-gray image) [22].
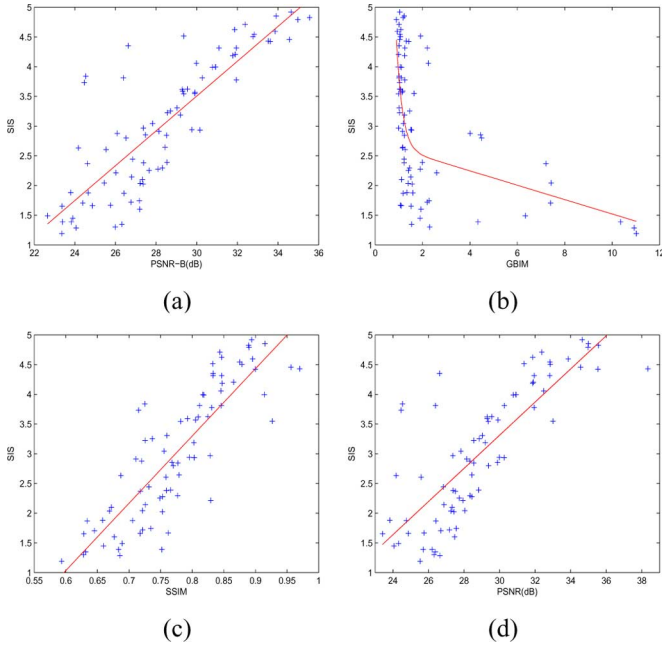

Fig. 9. Scatter plots of subjective impairment score (SIS) versus quality indices. (a) SIS versus PSNR: CC $= 0.8041$, RMSE $= 0.6607$, MAE $= 0.5131$. (b) SIS versus GBIM: CC $= 0.4774$, RMSE $= 0.8654$, MAE $= 0.7006$. (c) SIS versus SSIM: CC $= 0.8529$, RMSE $= 0.5802$, MAE $= 0.4765$. (d) SIS versus PSNR-B: CC $= 0.8442$, RMSE $= 0.5957$, MAE $= 0.4361$.

Fig. 10. Reconstructed images of Lena with quantization step 80. (a) No filter (PSNR $= 29.38$ dB, PSNR-B $= 26.52$ dB, SSIM $= 0.7700$, GBIM $= 4.494$). (b) POCS deblocking filter (PSNR $= 29.31$ dB, PSNR-B $= 29.31$ dB, SSIM $= 0.7926$, GBIM $= 1.161$).
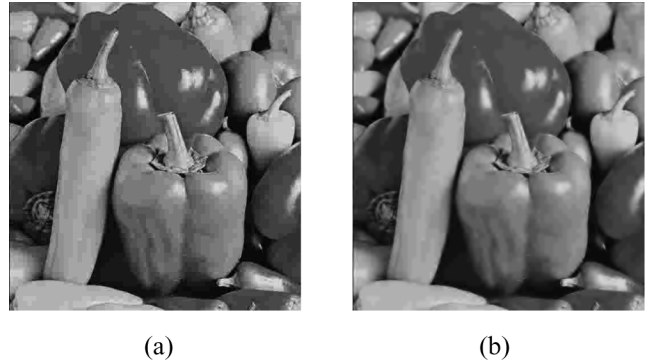

Fig. 11. Reconstructed images of Peppers with quantization step 80. (a) No filter (PSNR $= 29.88$ dB, PSNR-B $= 27.48$ dB, SSIM $= 0.7680$, GBIM $= 4.442$). (b) POCS deblocking filter (PSNR $= 29.91$ dB, PSNR-B $= 29.91$ dB, SSIM $= 0.8053$, GBIM $= 1.138$).

to the original image. The 80 test images were used in the subjective experiment: Lena, Peppers, Barbara, and Goldhill images with quantization steps 20, 40, 80, 120, and 160 for cases no-filter, 3×3 filter, 7×7, and POCS. The observers were recruited among junior and sophomore undergraduate students in a Signal Processing class at Konkuk University, Seoul (21 observers participated), and their scores were averaged for each test image.

A five-parameter logistic function was used in the nonlinear regression process (a logistic function with an added linear term) as in [3], [4]. Fig. 9 shows the scatter plots of subjective impairment score (SIS) versus quality indices. In Fig. 9, the line indicates the fitted curve by regression. We calculated three statistical values for performance comparison. The first value is the linear correlation coefficient (CC) between SIS and quality indices. The second and third values are root-mean-squared error (RMSE) and mean-absolute error (MAE) between the SIS and the fitted curve after nonlinear regression.

The blockiness-specific quality index, GBIM, gave relatively worse performance. The CC was much smaller, and the RMSE and MAE were larger, than for SSIM and PSNR-B. The SSIM and the proposed index, PSNR-B, resulted in better performance

compared to the conventional quality index PSNR in terms of CC, RMSE, and MAE. The performances of SSIM and PSNR-B were similar. The SSIM was slightly better in terms of CC and RMSE, while PSNR-B was better in terms of MAE.

G. Comparison of Quality Indices

Fig. 10 shows Lena reconstructed from compression using quantization step 80. When no filter was applied as in Fig. 10(a), annoying blocking artifacts are clearly visible. When the POCS deblocking filter was applied [Fig. 10(b)], the blocking effects were greatly reduced, resulting in better subjective quality. The PSNR index produced slightly lower values than on the no-filtered image. Conversely, the PSNR-B and SSIM quality indices produced larger values on the POCS filtered image.

Fig. 11 shows Peppers reconstructed from compression, also using quantization step 80. When no filter is applied as in Fig. 11(a), blocking artifacts are clearly visible, especially on the peppers. When the POCS deblocking filter was applied as in Fig. 11(b), the blocking effects were mostly removed, resulting in better subjective quality. The PSNR-B and SSIM quality indices produced larger values on the POCS filtered image, in agreement with observation.

Fig. 12 shows the reconstructed Barbara image with quantization step 80. Blocking artifacts are visible in the no-filtered
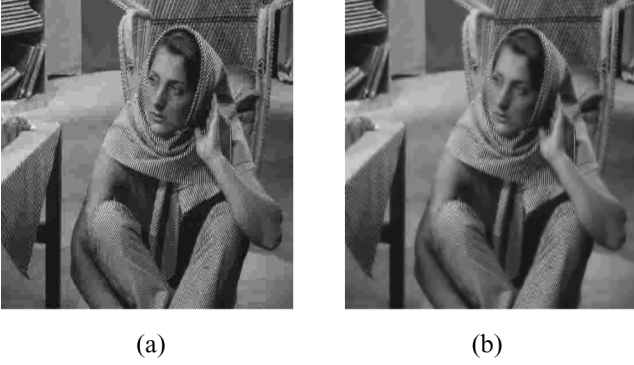
(a)   (b)

Fig. 12. Reconstructed images of Barbara with quantization step 80. (a) No filter (PSNR $=$ 27.94 dB, PSNR-B $=$ 26.02 dB, SSIM $=$ 0.8293, GBIM $=$ 2.602). (b) POCS deblocking filter (PSNR $=$ 27.37 dB, PSNR$-$B $=$ 27.37 dB, SSIM $=$ 0.8284, GBIM $=$ 0.990).

image and are mostly removed in the POCS filtered image. Again, PSNR produced slightly larger values on the no-filtered image, while the SSIM index was almost unchanged. PSNR-B produced slightly larger values on the POCS filtered image.

A number of observations may be made from these simulation results. First, the PSNR-B metric captures subjective quality on images containing blocking artifacts as well as deblocking artifacts. This is substantiated both by agreement with the perceptually significant SSIM index and by subjective quality assessment experiment. Second, the PSNR does not perform as well, as might be expected. Thirdly, both the PSNR-B and the SSIM index indicate that the POCS approach improves the perceptual quality of block degraded images more than does simple lowpass filtering. Fourth, the blockiness-specific GBIM has limitations for measuring image quality including blocking artifacts and deblocking artifacts, even though it is effective just for measuring the amount of blockiness.

VII. STUDY OF H.264 IN-LOOP FILTER

Now we present simulation results for deblocking filters for H.264 video coding. The H.264 encoding and decoding simulations are performed using the H.264 reference software in [18]. The in-loop deblocking filter is a key component in H.264 video coding. If the filter is selected by an encoding parameter, in-loop filtering is performed both in encoding and in decoding. If it is not selected, in-loop filtering is not performed either in encoding or in decoding. In H.264, the quantization step size is controlled by the quantization parameter (QP) during encoding [16]. The QP can take 52 values ranging from 0 to 51, and the quantization step is doubled for each increment of six in the QP [19]. In H.264 coding, the quantization step is the same for all transform coefficients as determined by the QP.

To assess the in-loop filter using the quality indices, the size of a group-of-pictures (GOP) is set as eight with one I-frame and seven P-frames. In the simulations, 16 frames are encoded and decoded. The quality indices were applied on the original (reference) and decoded images at each frame, and the quality scores were then averaged over the 16 frames.

(a)   (b)
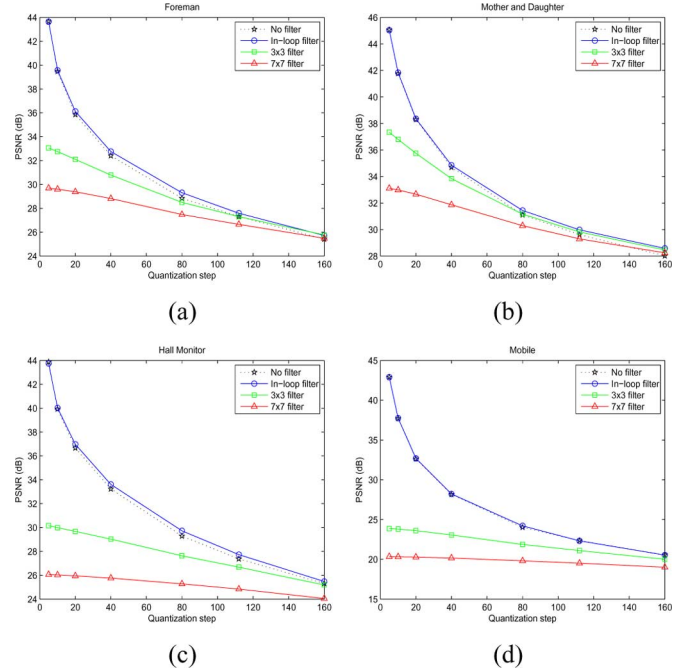
(c)   (d)

Fig. 13. PSNR comparison of filters for H.264 videos. (a) Foreman. (b) Mother and Daughter. (c) Hall Monitor. (d) Mobile.

A. PSNR Analysis

Fig. 13 examines the H.264 in-loop filter and lowpass filters using the PSNR as an analysis tool. The 3×3 and 7×7 lowpass filters do not provide improvement compared to not filtering for small to medium quantization step sizes ($\Delta \leq 80$). The lowpass filters produce slight improvement compared to not filtering for $\Delta = 160$ on the Foreman and Mother and Daughter videos. The in-loop filter gave a slight improvement of PSNR compared to not filtering for mid-to-large quantization steps ($\Delta \geq 40$) on the Foreman, Mother and Daughter, and Hall Monitor videos. The in-loop filter did not produce improvements compared to not filtering on the complex Mobile video, according to the PSNR. However, the PSNR is of dubious value when assessing perceptual quality.

B. SSIM Analysis

Fig. 14 studies the deblocking methods using the SSIM index [1]. The in-loop filter produced improvement in the SSIM values compared to not filtering for mid-to-large quantization steps ($\Delta \geq 40$) on the Foreman, Mother and Daughter, and Hall Monitor videos. As the quantization step was increased, the in-loop filter systematically produced larger SSIM values. The 3×3 filter also produced improvement according to SSIM as compared to not filtering on the Foreman, Mother and Daughter, and Hall Monitor videos, when the quantization step was greater than 40. For the Mobile video, the in-loop filter produced SSIM values almost the same as those for not filtering while the lowpass filters gave lower SSIM values. This is clear evidence that the in-loop filter works well, according to the perceptually relevant SSIM index.
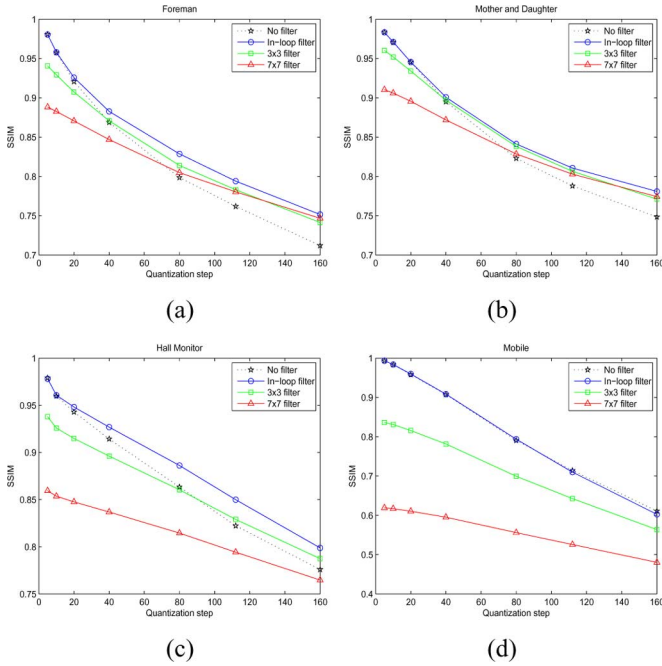
Fig. 14. SSIM comparison of filters for H.264 videos. (a) Foreman. (b) Mother and Daughter. (c) Hall Monitor. (d) Mobile.

Fig. 15. PSNR-B comparison of filters for H.264 videos. (a) Foreman. (b) Mother and Daughter. (c) Hall Monitor. (d) Mobile.

C. PSNR-B Analysis

Fig. 15 analyzes the in-loop filter using PSNR-B. PSNR-B produces trends similar to SSIM and visual analysis, while the PSNR shows different trends. For mid-to-large quantization steps ($\Delta \geq 80$), PSNR-B shows that the in-loop filter delivers marginal improvement as compared to not filtering, while the PSNR shows little change on the Foreman, Mother and Daughter, and Hall Monitor videos. For a large quantization step $\Delta = 160$, the PSNR-B comparison in Fig. 15 shows that the 3×3 and 7×7 filters deliver improvements, while the PSNR comparison in Fig. 13 does not.

D. Analysis Using Quality Indices

Fig. 16 shows the decoded I-frame from Foreman video when the QP is 42, which corresponds to a quantization step (Δ) of 80. The subjective quality produced by the in-loop filter is noticeably better than for the no-filter case. The PSNR-B for the in-loop filter is marginally higher than for no-filter (by 2.81 dB), while the PSNR values are very similar with a difference of 0.52 dB. The SSIM value for the in-loop filter result is higher than the no-filter result by 0.0341. This difference is visible in Fig. 14(a).

Fig. 17 shows the decoded I-frame from Mother and Daughter video for $QP = 42$ ($\Delta = 80$). The blocking artifacts are noticeably reduced and the subjective quality is nicely improved using the in-loop filter. The PSNR-B of the in-loop filter result is higher by 2.72 dB, while the PSNR is higher by just 0.32 dB The SSIM value increased by 0.0178, which is visible in Fig. 14(b).

Overall the in-loop filter generally resulted in improvements compared to no-filter when the quantization step was large, but did not give noticeable improvements when the quantization step was small or the scene was complex as the Mobile. Since
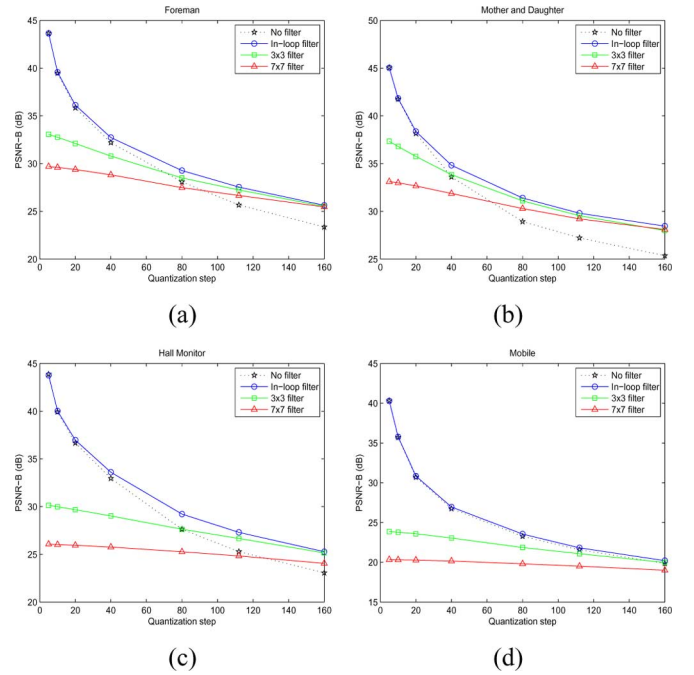

Fig. 16. H.264 decoded I-frame from Foreman video ($QP = 42$, $\Delta = 80$). (a) No filter ($PSNR = 29.19$ dB, $PSNR\text{-}B = 26.63$ B, $SSIM = 0.8041$). (b) In-loop filter ($PSNR = 29.71$ dB, $PSNR\text{-}B = 29.44$ dB, $SSIM = 0.8382$).

Fig. 17. H.264 decoded I-frame from Mother and Daughter video ($QP = 42$, $\Delta = 80$). (a) No filter ($PSNR = 31.07$ dB, $PSNR\text{-}B = 28.64$ dB, $SSIM = 0.8232$). (b) In-loop filter ($PSNR = 31.39$ dB, $PSNR\text{–}B = 31.36$ dB, $SSIM = 0.8410$).

the in-loop filter does not give improvements in many cases and the implementation cost is high as discussed in [23], the inclusion of in-loop filter should be selected carefully in real applications.

VIII. Concluding Remarks

We proposed the block-sensitive image quality index PSNR-B for quality assessment of deblocked images. It modifies the conventional PSNR by including an effective blocking effect factor. In simulations, we compared relevant image quality indices for deblocked images. The simulation results show that PSNR-B results in better performance than PSNR for image quality assessment of these impaired images. By comparison, the blockiness-specific index GBIM effectively assesses blockiness, but has limitations for image quality assessment. PSNR-B shows similar trends with the perceptually proven index SSIM. It is attractive since it is specific for assessing image quality, specifically the severity of blocking artifacts. The PSNR-B takes values in a similar range as PSNR and is, therefore, intuitive for users of PSNR, while it results in better performance for quality assessment of deblocked images.

For future work, we look forward to new problems to solve in this direction of inquiry. Firstly, quality studies of this type using special-purpose quality indices (such as PSNR-B) and perceptually proven indices (such SSIM) in conjunction are of considerable value, not only for studying deblocking operations, but also for other image improvement applications, such as restoration, denoising, enhancement, and so on. Second, we envision that nonlinear deblocking approaches could be developed using perceptual quality indices, such as SSIM, as optimized objective functions—such an approach may produce impressive results, as has occured in the linear restoration problem [25], and the image denoising problem [26]. A further application of interest is foveated image quality assessment [27], since certain methods of foveation can produce blocking artifacts [28]–[30].

References

[1] Z. Wang, A. C. Bovik, H. R. Sheikh, and E. P. Simoncelli, "Image quality assessment: From error visibility to structural similarity," *IEEE Trans. Image Process.*, vol. 13, no. 4, pp. 600–612, Apr. 2004.

[2] Z. Wang, E. P. Simoncelli, and A. C. Bovik, "Multi-scale structural similarity for image quality assessment," in *Proc. IEEE Asilomar Conf. Signal Syst. Comput.*, Nov. 2003.

[3] H. R. Sheikh and A. C. Bovik, "Image information and visual quality," *IEEE Trans. Image Process.*, vol. 15, no. 2, pp. 430–444, Feb. 2006.

[4] H. R. Sheikh and A. C. Bovik, "A statistical evaluation of recent full reference image quality assessment algorithms," *IEEE Trans. Image Process.*, vol. 15, no. 11, pp. 3441–3452, Nov. 2006.

[5] Z. Wang and A. C. Bovik, "A universal image quality index," *IEEE Signal Process. Lett.*, vol. 9, no. 3, pp. 81–84, Mar. 2002.

[6] B. Girod, "What's wrong with mean-squared error," in *Digital Images and Human Vision*, A. B. Watson, Ed. Cambridge, MA: MIT Press, 1993, pp. 207–220.

[7] Y. Yang, N. P. Galatsanos, and A. K. Katsaggelos, "Projection-based spatially adaptive reconstruction of block-transform compressed images," *IEEE Trans. Image Process.*, vol. 4, no. 7, pp. 896–908, Jul. 1995.

[8] Y. Yang, N. P. Galatsanos, and A. K. Katsaggelos, "Regularized reconstruction to reduce blocking artifacts of block discrete cosine transform compressed images," *IEEE Trans. Circuits Syst. Video Technol.*, vol. 3, no. 6, pp. 421–432, Dec. 1993.

[9] H. Paek, R.-C. Kim, and S. U. Lee, "On the POCS-based postprocessing technique to reduce the blocking artifacts in transform coded images," *IEEE Trans. Circuits Syst. Video Technol.*, vol. 8, no. 3, pp. 358–367, Jun. 1998.

[10] S. H. Park and D. S. Kim, "Theory of projection onto narrow quantization constraint set and its applications," *IEEE Trans. Image Process.*, vol. 8, no. 10, pp. 1361–1373, Oct. 1999.

[11] A. Zakhor, "Iterative procedure for reduction of blocking effects in transform image coding," *IEEE Trans. Circuits Syst. Video Technol.*, vol. 2, no. 1, pp. 91–95, Mar. 1992.

[12] Y. Jeong, I. Kim, and H. Kang, "A practical projection-based postprocessing of block-coded images with fast convergence rate," *IEEE Trans. Circuits and Syst. Video Technol.*, vol. 10, no. 4, pp. 617–623, Jun. 2000.

[13] S. Liu and A. C. Bovik, "Efficient DCT-domain blind measurement and reduction of blocking artifacts," *IEEE Trans. Circuits Syst. Video Technol.*, vol. 12, no. 12, pp. 1139–1149, Dec. 2002.

[14] Z. Wang and A. C. Bovik, "Blind measurement of blocking artifacts in images," in *Proc. IEEE Int. Conf. Image Process.*, Vancouver, Canada, Oct. 2000, pp. 981–984.

[15] P. List, A. Joch, J. Laimena, J. Bjøntegaard, and M. Karczewicz, "Adaptive deblocking filter," *IEEE Trans. Circuits Syst. Video Technol.*, vol. 13, no. 7, pp. 614–619, Jul. 2003.

[16] *Draft ITU-T Recommendation and Final Draft International Standard of Joint Video Specification (ITU Rec. H.264—ISO/IEC 14496-10 AVC)*, , 2003, Doc.JVT-G050.

[17] T. Wiegand, G. Sullivan, J. Bjøntegaard, and G. A. Luthra, "Overview of the H.264/AVC video coding standard," *IEEE Trans. Circuits Syst. Video Technol.*, vol. 13, no. 7, pp. 560–576, Jul. 2003.

[18] H.264/AVC Software Co-ordination [Online]. Available: http://iphome.hhi.de/suehring/tml/index.htm

[19] I. E. G. Richardson, *H.264 and MPEG-4 Video Compression*. Hoboken, NJ: Wiley, 2003.

[20] H. R. Wu and M. Yuen, "A generalized block-edge impairment metric for video coding," *IEEE Signal Process. Lett.*, vol. 4, no. 11, pp. 317–320, Nov. 1997.

[21] G. Zhai, W. Zhang, X. Yang, W. Lin, and Y. Xu, "No-reference noticeable blockiness estimation in images," *Signal Process. Image Commun.*, vol. 23, pp. 417–432, 2008.

[22] "Methodology for the subjective assessment of the quality of television pictures," 2002, Recommendation ITU-R BT.500-11.

[23] Y. Zhong, I. Ricardson, A. Miller, and Y. Zhao, "Perceptual quality of H.264/AVC de-blocking filter," *IEE VIE*, pp. 379–384, Apr. 2005.

[24] *The Handbook of Image and Video Processing*, A. C. Bovik, Ed., 2nd ed. New York: Morgan Claypool, 2005.

[25] S. S. Channappayya, A. C. Bovik, C. Caramanis, and R. W. Heath, Jr, "Design of linear equalizers optimized for the structural similarity index," *IEEE Trans. Image Process.*, vol. 17, no. 6, pp. 857–872, Jun. 2008.

[26] S. S. Channappayya, A. C. Bovik, and R. W. Heath, Jr, "Perceptual soft thresholding using the structural similarity index," in *Proc. IEEE Int. Conf. Image Process.*, San Diego, CA, Oct. 2008, pp. 569–572.

[27] S. Lee, M. S. Pattichis, and A. C. Bovik, "Foveated video quality assessment," *IEEE Trans. Multimedia*, vol. 4, no. 1, pp. 129–132, Mar. 2002.

[28] W. N. Klarquist and A. C. Bovik, "A foveated, multi-fixation, vergent active stereo system for dynamic three-dimensional scene recovery," *IEEE Trans. Robot. Autom.*, vol. 14, no. 5, pp. 755–770, Oct. 1998.

[29] S. Lee, M. S. Pattichis, and A. C. Bovik, "Foveated video compression with optimal rate control," *IEEE Trans. Image Process.*, vol. 10, no. 7, pp. 977–992, Jul. 2001.

[30] Z. Wang, L. Lu, and A. C. Bovik, "Foveation scalable video coding with automatic fixation selection," *IEEE Trans. Image Process.*, vol. 12, no. 2, pp. 243–254, Feb. 2003.

Changhoon Yim (M'91) received the B.Eng. degree from the Department of Control and Instrumentation Engineering, Seoul National University, Korea, in 1986, the M.S. degree in electrical engineering from Korea Advanced Institute of Science and Technology, Korea, in 1988, and the Ph.D. degree in electrical and computer engineering from the University of Texas, Austin, in 1996.

He is currently an Associate Professor in the Department of Internet and Multimedia Engineering, Konkuk University, Seoul, Korea. He was a Research Engineer working on HDTV at the Korean Broadcasting System, Korea, from 1988 to 1991. From 1996 to 1999, he was a Member of technical staff in HDTV and Multimedia Division, Sarnoff Corporation, Princeton, NJ. From 1999 to 2000, he worked at Bell Labs, Lucent Technologies, Murray Hill, NJ. From 2000 to 2002, he was a Software Engineer in KLA-Tencor Corporation, Milipitas, CA. From 2002 to 2003, he was a Principal Engineer at Samsung Electronics, Suwon, Korea. His research interests include digital image processing, video compression, and multimedia communication.

Alan Conrad Bovik (S'80–M'81–SM'89–F'96) received the B.S., M.S., and Ph.D. degrees in electrical and computer engineering from the University of Illinois at Urbana-Champaign, Urbana, in 1980, 1982, and 1984, respectively.

He is currently the Curry/Cullen Trust Endowed Professor at The University of Texas at Austin, where he is the Director of the Laboratory for Image and Video Engineering (LIVE) in the Center for Perceptual Systems. His research interests include image and video processing, computational vision, digital microscopy, and modeling of biological visual perception. He has published over 450 technical articles in these areas and holds two U.S. patents. He is also the author of *The Handbook of Image and Video Processing* (Elsevier, 2005, 2nd ed.) and *Modern Image Quality Assessment* (Morgan & Claypool, 2006).

Dr. Bovik has received a number of major awards from the IEEE Signal Processing Society, including: the Education Award (2007); the Technical Achievement Award (2005); the Distinguished Lecturer Award (2000); and the Meritorious Service Award (1998). He is also a recipient of the Distinguished Alumni Award from the University of Illinois at Urbana-Champaign (2008), the IEEE Third Millennium Medal (2000), and two journal paper awards from the International Pattern Recognition Society (1988 and 1993). He is a Fellow of the Optical Society of America and the Society of Photo-Optical and Instrumentation Engineers. He has been involved in numerous professional society activities, including: Board of Governors, IEEE Signal Processing Society, 1996–1998; Editor-in-Chief, IEEE TRANSACTIONS ON IMAGE PROCESSING, 1996–2002; Editorial Board, PROCEEDINGS OF THE IEEE, 1998–2004; Series Editor for Image, Video, and Multimedia Processing, Morgan and Claypool Publishing Company, 2003–present; and Founding General Chairman, First IEEE International Conference on Image Processing, Austin, TX, November 1994. He is a registered Professional Engineer in the State of Texas and is a frequent consultant to legal, industrial, and academic institutions.